Applied Energy 148 (2015) 105–114

Contents lists available at ScienceDirect

Applied Energy

journal homepage: www.elsevier.com/locate/apenergy

Comparison of different heat transfer models for parabolic trough solar collectors

Hongbo Liang, Shijun You, Huan Zhang *

School of Environmental Science and Engineering, Tianjin University, Tianjin, China

HIGHLIGHTS

- We summarized different assumptions and details for 1-D math models of PTC.
- All the heat transfer processes were considered.
- It can choose an appropriate 1-D model under a certain condition due to this paper.
- A simple algorithm was adopted to make control equations linear and solve easily.
- 1-D model is precise and simple enough compared with 3-D model by comparison.

ARTICLE INFO

Article history:
Received 27 November 2014
Received in revised form 10 March 2015
Accepted 11 March 2015
Available online 28 March 2015

Keywords:
Parabolic trough solar collector
Heat transfer model
Thermal performance research
Numerical simulation
Precision analysis

ABSTRACT

Parabolic trough solar collector (PTC) is one of the solar thermal energy applications, which focuses sunlight to heat the heat transfer fluid (HTF) circulating through the receiver. Researchers have put forward several heat transfer models for PTCs, basing on laws of conservation. This paper summarized the one-dimensional (1-D) mathematical models under different assumptions and details for PTCs. All the heat transfer processes were considered: convection within the absorber, in the annulus and between the glass and ambient; conduction through glass cover, absorber and support brackets; radiation in the annulus and from the glass to the sky. Moreover, a simple algorithm was adopted to make the control equations linear and solve easily. The difference in accuracy for diverse 1-D models were presented and analyzed on the basis of the experimental data from Sandia National Laboratories. The 1-D models with various details were different in accuracy and complexity. It can choose an appropriate 1-D model under a certain condition, which can be used in investigating the thermal performance of a PTC. In addition, the most accurate 1-D model presented in this paper were precise enough compared with the three-dimensional (3-D) model from other paper. The average difference of outlet temperature between the most accurate simulation in this paper and test data was 0.65 °C, however it was 2.69 °C between the 3-D model and experiment results. The reason may be that there were more assumptions for 3-D models than 1-D models, therefore the error was bigger.

© 2015 Elsevier Ltd. All rights reserved.

1. Introduction

A PTC focuses direct solar radiation onto the absorber located on its focal line. By circulating through the receiver, the HTF absorbs the concentrated solar thermal energy to raise its enthalpy (see Fig. 1). The application of PTCs can be divided into two major groups. One is Concentrated Solar Power (CSP) plants with the fluid temperature from 300 °C to 400 °C. The other supplies a temperature between 100 °C and 250 °C for domestic hot water, space heating and heat-driven refrigeration, etc. [1].

Many scholars have developed mathematical models for the PTC to study the heat transfer characteristics and improve its thermal performance. Dudley et al. [2] tested a SEGS LS-2 PTC with the black chrome and cermet coating under vacuum or air in the annulus, and bare receiver. Numerous papers quoted their experiment results to validate the theoretical models. Taken the thermal performances of different working oils into consideration, Ouagued et al. [3] proposed a 1-D model dividing the HCE into several segments for PTCs. Padilla et al. [4] established control equations for fluid, absorber and glass. Meanwhile, improvements in radiative heat transfer analysis were presented. Both 1-D and 2-D models were built in [5]: the 2-D model discretized the receiver into "N" segments along the length, the 1-D model did opposite. Almost all the physical

* Corresponding author. Tel./fax: +86 22 2789 2626.
E-mail address: zhhuan@tju.edu.cn (H. Zhang).

http://dx.doi.org/10.1016/j.apenergy.2015.03.059
0306-2619/© 2015 Elsevier Ltd. All rights reserved.

Q	heat transfer capacity (W)
W	solar irradiation absorption (W)
c_p	specific heat (J kg^{-1} K^{-1})
t	temperature (K)
t_{b0}	temperature of the fin base (K)
h	enthalpy (J kg^{-1}), convection heat transfer coefficient (W m^{-2} K^{-1})
g	gravity acceleration (m s^{-2})
z	altitude (m)
RT	source term (W m^{-3})
v	speed (m s^{-1})
x	axial direction
V	volume (m^3)
l	axial length of the receiver (m)
l_b	focal length (m)
d	diameter (m)
Nu	Nusselt number
Re	Reynolds number
Pr	Prandtl number
f	friction factor
Ra	Rayleigh number
$b_{r\text{-}g}$	interaction coefficient
$P_{r\text{-}g}$	annulus gas pressure (mm Hg)
k	mean-free-path between collisions of a molecule (cm)
A	area (m^2)
F	view factor
U	perimeter (m)
K	incident angle modifier
I	solar irradiation heat (W)
R	coefficient matrix
T	temperature matrix
M	constant matrix

Greek symbols

ρ	density (kg m^{-3})
ρ_c	reflectivity of the mirror
ε	emissivity
τ	time (s)
τ_g	transmissivity of the glass
λ	thermal conductivity (W m^{-1} K^{-1})
Δ	incremental value
α	accommodation coefficient
$\alpha_{g\text{-}a}$	thermal diffusivity (m^2 s^{-1})
α_g	glass absorptivity for solar irradiation
α_r	absorber absorptivity for solar irradiation
γ	ratio of specific heats for the annulus gas
δ	molecular diameter of annulus gas (cm)
σ	Stefan Boltzmann constant (5.67 $\times$ 10^{-8} W m^{-2} K^{-4})
ν	kinematic viscosity (m^2 s^{-1})
β	volumetric thermal expansion coefficient (K^{-1})
η	efficiency
μ	dynamic viscosity (Pa s)

Subscripts

f	heat transfer fluid
r	absorber
g	glass cover
a	air
s	sky
b	support bracket
in	inner surface
ou	outer surface
$conv$	convection
$cond$	conduction
rad	radiation
p	plug into the absorber
i	node i
j	node j
std	standard temperature and pressure

Abbreviations

PTC	parabolic trough solar collector
1-D	one-dimensional
2-D	two-dimensional
3-D	three-dimensional
HCE	heat collection element
HTF	heat transfer fluid

parameters related to the model were discussed in it, as well as the model assumptions, limitations and proposals for improvement. Kalogirou et al. [6] considered conduction through the absorber pipe and glass cover at the same time in modeling. Odeh et al. [7] developed a model based on the absorber wall temperature, which can evaluate the collector performance with various kinds of working fluids. Kassem [8] simulated numerically the natural convection heat transfer between the absorber and glass envelope. A conclusion that the heat transfer can be optimized with a suitable eccentricity had been drawn. Li et al. [9] presented the hydrogen permeation model for PTCs. The least squares support vector machine (LSSVM) method was established to model and optimize the PTC system [10]. Gong et al. [11] combined an optimized 1-D model with a 3-D end model for PTCs, which showed a good accordance with the test data. Lu et al. [12] developed a non-uniform thermal model, both absorber and glass being divided into two regions for uneven solar radiation and temperature. He et al. analyzed the complicated coupled heat transfer process in PTC system by combination of Monte Carlo Ray Trace (MCRT) and Finite Volume Method (FVM) [13]. They proposed a more-detailed 3-D model [14]. Wu et al. [15] considered the non-uniform temperature distribution in their model, which was required to identify the causation of parabolic trough receiver's failure.

Various heat transfer mathematical models established by different scholars were not exactly the same although they were all based on energy balance. This paper summarized these 1-D mathematical models under different assumptions and details for PTCs. All the heat transfer processes have been discussed. In order to find the key to the accuracy of models, the simulated data were analyzed and validated with experimental data from Sandia National Laboratories [2]. A simple algorithm for solving the control equations was adopted. The 1-D models with diverse details were different in accuracy and complexity. A 1-D model may be more accurate, but more complicated. We can choose an appropriate 1-D model to investigate the thermal performance of PTCs under a certain condition. In addition, the most accurate 1-D model in this paper was compared with a 3-D model from other paper [13].

2. Heat transfer model

2.1. HCE introduction

HCE is a core component of a PTC, as shown in Fig. 2. It consists of an absorber pipe surrounded by a glass cover with bellows at each end. The annulus space between them is usually vacuum to reduce heat loss. The absorber is a metallic tube with a selective coating that has high absorptivity for solar radiation but low emissivity in long wave energy spectrum, and this can decrease thermal radiation loss. Thermal resistance of the selective coating is negligible for simplification [5]. The getter is used to absorb

hydrogen between the annulus, and the bellows can coordinate the difference of thermal expansion between glass and metal, thus reducing heat loss.

2.2. Physical model

Solar radiation is the energy source for a HCE (see Fig. 3). The system temperature begins to rise as the absorber tube absorbs solar energy Wr reflected by the mirror. Under the effect of temperature difference, the absorber tube exchanges heat with the working fluid by forced convection $Q_{r\text{-}f.conv}$ and with the glass envelope by convection $Q_{r\text{-}g.conv}$ and radiation $Q_{r\text{-}g.rad}$. In addition, the absorber tube losses heat to environment by conduction $Q_{r\text{-}b.cond}$ in the junction with the support brackets (see Fig. 1). The glass cover also absorbs solar radiation W_g although the absorptivity of glass is small. Along with heat transferred from the absorber, the glass tube losses heat to surrounding air by convection $Q_{g\text{-}a.conv}$ and to sky by radiation $Q_{g\text{-}s.rad.}$

2.3. 1-D mathematical model

2.3.1. Model assumptions and control equations

The common heat transfer models for a PTC are on the law of conservation of energy. The energy partial differential equation is usually described in Eq. (1): transient term + convection = conduction + source term:

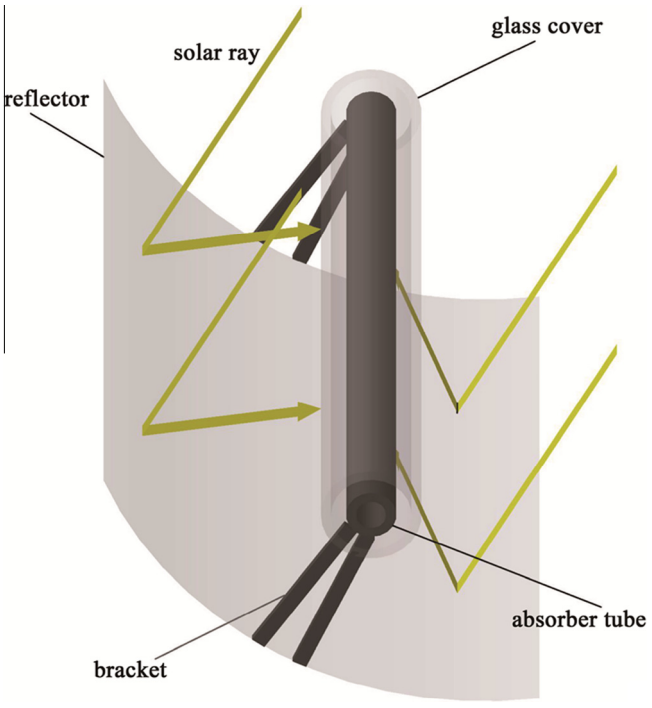

Fig. 1. Schematic of a PTC.

$$\frac{\partial(\rho c_p t)}{\partial \tau} + div\left[\rho \vec{v}\left(h + \frac{v^2}{2} + gz\right)\right] = div[\lambda grad(t)] + RT \tag{1}$$

In this paper, some assumptions are made: (a) The change of kinetic and potential energy is negligible and enthalpy $h \approx c_p t$. (b) The thermophysical parameters for each control volume are represented by its central point. (c) It is steady state. (d) The 1-D model is discretized (see Fig. 4) along the axis direction by central difference shown in Eqs. (2) and (3).

$$\frac{\partial t}{\partial x} = \frac{t_{i+1} - t_{i-1}}{2\Delta x} \tag{2}$$

$$\frac{\partial^2 t}{\partial x^2} = \frac{t_{i+1} - 2t_i + t_{i-1}}{\Delta x^2} \tag{3}$$

Three control volumes are considered for 1-D model in this paper: glass cover, absorber and working fluid. The convection term for the glass tube and the absorber tube is equal to zero. The governing equation of each control volume is represented as below:

For glass cover:

$$0 = \lambda_{g.i}\frac{t_{g.i+1} - 2t_{g.i} + t_{g.i-1}}{\Delta x^2} + (W_{g.i} + Q_{r\text{-}g.conv.i} + Q_{r\text{-}g.rad.i} - Q_{g\text{-}a.conv.i} - Q_{g\text{-}s.rad.i})/\Delta V_{g.i} \tag{4}$$

For absorber tube:

$$0 = \lambda_{r.i}\frac{t_{r.i+1} - 2t_{r.i} + t_{r.i-1}}{\Delta x^2} + (W_{r.i} - Q_{r\text{-}g.conv.i} - Q_{r\text{-}g.rad.i} - Q_{r\text{-}f.conv.i} - Q_{r\text{-}b.cond.i})/\Delta V_{r.i} \tag{5}$$

For heat transfer fluid:

$$\rho_{f.i}c_{p.f.i}v_{f.i}\frac{t_{f.i+1} - t_{f.i-1}}{2\Delta x} = \lambda_{f.i}\frac{t_{f.i+1} - 2t_{f.i} + t_{f.i-1}}{\Delta x^2} + Q_{r\text{-}f.conv.i}/\Delta V_{f.i} \tag{6}$$

2.3.2. Single-value conditions

2.3.2.1. Geometrical conditions. In this paper, the simulated results are compared with the experimental data generated from Sandia National Laboratories [2], and Table 1 gives the specifications for the PTC.

2.3.2.2. Physical conditions. The working liquid oil used in the experiment is Syltherm 800, whose specific heat $c_{p.f.i}$ (J kg^{-1} K^{-1}), density $\rho_{f.i}$ (kg m^{-3}), thermal conductivity $\lambda_{f.i}$ (W m^{-1} K^{-1}), and dynamic viscosity $\mu_{f.i}$ (Pa s) are shown in Eqs. (7)–(10) [14] (temperature range from 373.15 K to 673.15 K).

$$c_{p.f.i} = 1107.798 + 1.708t_{f.i} \tag{7}$$

$$\rho_{f.i} = 1105.702 - 0.4153495t_{f.i} - 6.061657 \times 10^{-4}t_{f.i}^2 \tag{8}$$

$$\lambda_{f.i} = 0.190021 - 1.875266 \times 10^{-4}t_{f.i} - 5.753496 \times 10^{-10}t_{f.i}^2 \tag{9}$$

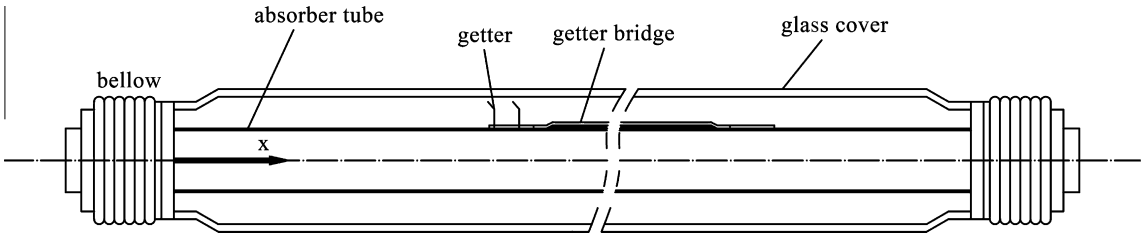

Fig. 2. Schematic of a HCE [5].

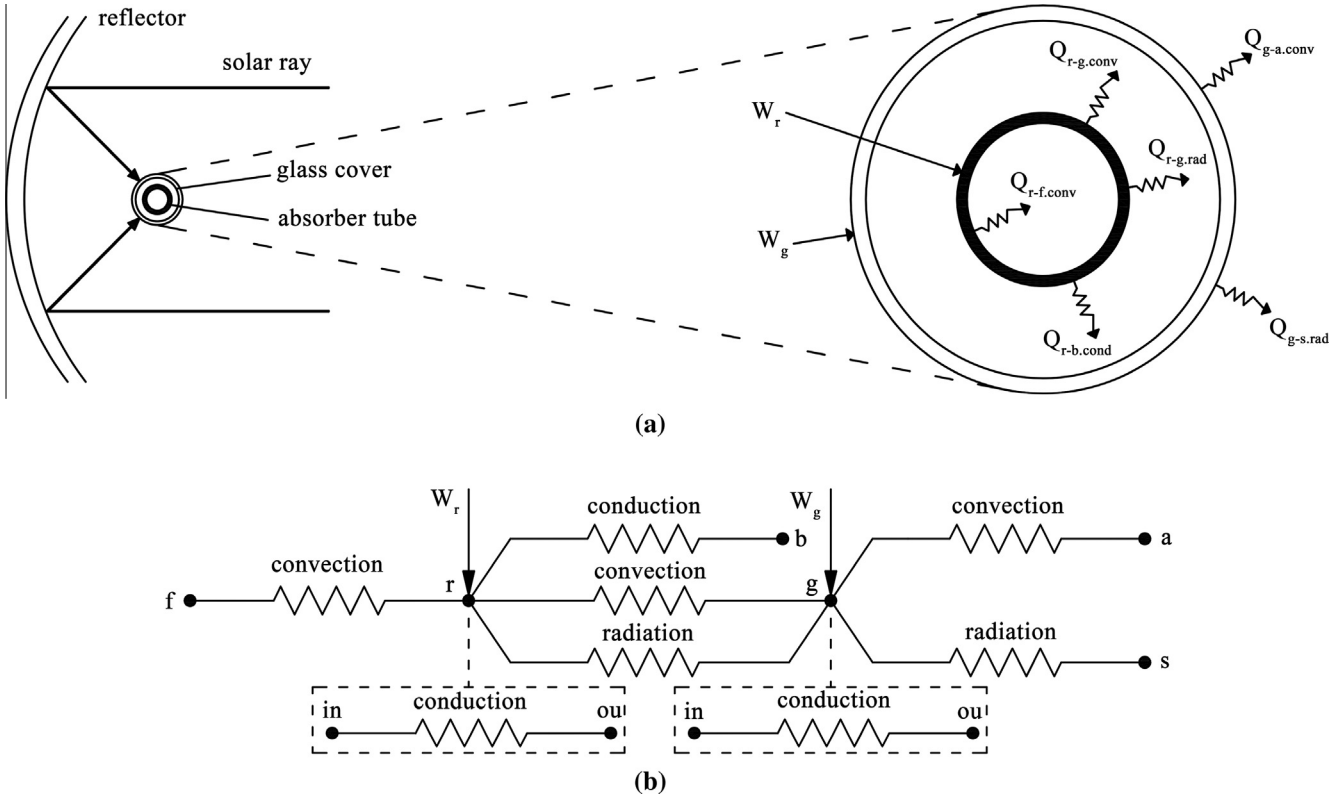

Fig. 3. Heat transfer schematic of a cross section (a) and network of thermal resistance (b).

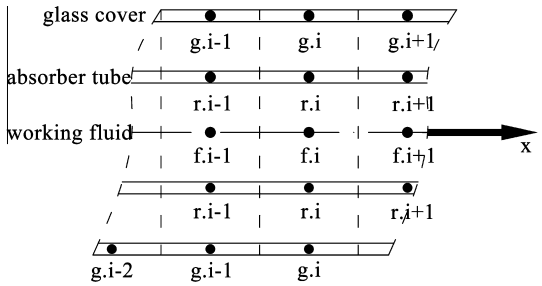

Fig. 4. The 1-D model along the receiver axis direction.

$$\mu_{f.i} = 0.08486612 - 5.541277 \times 10^{-4} t_{f.i} + 1.388285 \times 10^{-6} t_{f.i}^2 - 1.566003 \times 10^{-9} t_{f.i}^3 + 6.672331 \times 10^{-13} t_{f.i}^4 \quad (10)$$

2.3.2.3. Initial conditions. The initial conditions are not considered due to the steady-state heat transfer model in this paper.

2.3.2.4. Boundary conditions. Working fluid inlet temperature is the first kind thermal boundary condition, the solar irradiation absorption is the second one, and the environmental temperature is the third one. For glass tube and absorber pipe, their ends are adiabatic. For heat transfer media, its inlet speed is the velocity boundary condition.

2.4. Heat transfer interactions calculation

2.4.1. Convection heat transfer between the fluid and the absorber

The convection heat transfer between the fluid and the absorber inner surface is usually calculated by the Newton cooling law:

Table 1
Specifications for the PTC [2,3,16].

Module size	7.8 m × 5 m (as tested at Sandia)
Rim angle	70°
Aperture area	39.2 m^2 (as tested at Sandia)
Focal length	1.84 m
Concentration ratio	71
Absorber length	4 m (2 per module at Sandia)
Absorber inner diameter	0.066 m
Absorber outer diameter	0.070 m
Glass tube inner diameter	0.109 m
Glass tube outer diameter	0.115 m

$$Q_{r\text{-}f.conv.i} = \pi d_{r\text{-}in} \Delta l h_{r\text{-}f.conv.i} (t_{r.i} - t_{f.i}) \quad (11)$$

and the convective heat transfer coefficient $h_{r\text{-}f.conv.i}$ is given by:

$$h_{r\text{-}f.conv.i} = \frac{Nu_{r\text{-}f.i} \lambda_{f.i}}{d_{r\text{-}in}} \quad (12)$$

The Nusselt number $Nu_{r\text{-}f.i}$ is based on the inner diameter of the absorber $d_{r\text{-}in,}$ but it is substituted by the hydraulic diameter of $d_{r\text{-}in} - d_p$ for annulus flow. For 1-D model, $t_{r.i}$ and $t_{f.i}$ are independent in circumferential and radial direction.

As the Reynolds number $Re_{f.i}$ is lower than 2300, it's laminar flow and the $Nu_{r\text{-}f.i}$ is constant. For the experiment in [2], the $Nu_{r\text{-}f.i}$ is approximately 5.22 [5].

For transitional and turbulent flow, the correlation [3–6,17] is written as:

$$Nu_{r\text{-}f.i} = \frac{f_{r.i}/8 (Re_{f.i} - 1000) Pr_{f.i}}{1 + 12.7 \sqrt{f_{r.i}/8} (Pr_{f.i}^{2/3} - 1)} \left(\frac{Pr_{f.i}}{Pr_{r.i}} \right)^{0.11} \quad (13)$$

with

$$f_{r.i} = (1.82 \log_{10}(Re_{f.i}) - 1.64)^{-2} \quad (14)$$

For $0.5 < Pr_{f.i} < 2000$ and $2300 < Re_{f.i} < 5 \times 10^6$

All the fluid properties are calculated based on $t_{f.i}$ except $Pr_{r.i}$ depending on the temperature of absorber inner surface. In addition, the smooth inner surface is assumed.

2.4.2. Heat transfer between the absorber and the glass

The heat transfer mechanism between the absorber tube and the glass cover includes convection and radiation.

The convection heat loss depends on the pressure in the annulus. At low pressure, the convection mechanism is molecular conduction, while it is free convection at higher pressure. Different researches adopted diverse pressure demarcation point, which was 133.3 Pa in [5], whereas 0.013 Pa in [6] for example. In this paper, 0.013 Pa is the dividing point between the low and high pressure.

In common 1-D models, radiation between adjacent nodes was not considered in some papers, but was done in others such as in [4]. It's one of the important influence factors for improving calculation precision and analyzed below.

2.4.2.1. Convection heat transfer. The convection heat transfer between the absorber pipe outer surface and the glass tube inner surface can be expressed as below:

$$Q_{r\text{-}g.conv.i} = \pi d_{r\text{-}ou} \Delta l h_{r\text{-}g.conv.i} (t_{r.i} - t_{g.i}) \tag{15}$$

(A) Vacuum in annulus

When pressure in the annulus is lower than 0.013 Pa, the heat transfer coefficient $h_{r\text{-}g.conv.i}$ is given by [6,16,18]:

$$h_{r\text{-}g.conv.i} = \frac{\lambda_{std.i}}{d_{r\text{-}ou}/2\ln(d_{g\text{-}in}/d_{r\text{-}ou}) + b_{r\text{-}g} k_i (d_{r\text{-}ou}/d_{g\text{-}in} + 1)} \tag{16}$$

$$b_{r\text{-}g} = \frac{(2\text{-}\alpha)(9\gamma - 5)}{2\alpha(\gamma + 1)} \tag{17}$$

$$k_i = \frac{2.331 \times 10^{-20} t_{r\text{-}g.i}}{P_{r\text{-}g} \delta^2} \tag{18}$$

For $Ra_{g\text{-}in.i} < (d_{g\text{-}in}/(d_{g\text{-}in} - d_{r\text{-}ou}))^4$

where $t_{r\text{-}g.i}$ = average temperature $(t_{r.i} + t_{g.i})/2$.

As shown in [6,16,19], the accommodation coefficient is fixed to one in this research. When the gas of annulus is air, the average temperature is 573.15 K and the pressure is 0.013 Pa, the mean-free-path between collisions of a molecule equals to 88.67 cm, ratio of specific heats for annulus gas equals to 1.39, and molecular diameter of annulus gas equals to 3.53×10^{-8} cm.

(B) Pressure in annulus

When pressure in the annulus is higher than 0.013 Pa, the heat transfer mechanism is natural convection and $h_{r\text{-}g.conv.i}$ is evaluated as [16,20]:

$$h_{r\text{-}g.conv.i} = \frac{2\lambda_{eff.i}}{d_{r\text{-}ou}\ln(d_{g\text{-}in}/d_{r\text{-}ou})} \tag{19}$$

$$\frac{\lambda_{eff.i}}{\lambda_{r\text{-}g.i}} = 0.386 \left(\frac{Pr_{r\text{-}g.i}}{0.861 + Pr_{r\text{-}g.i}} \right)^{0.25} Ra_{C.i}^{0.25} \tag{20}$$

$$Ra_{C.i} = \frac{\ln(d_{g\text{-}in}/d_{r\text{-}ou})^4}{L_C^3 (d_{r\text{-}ou}^{-0.6} + d_{g\text{-}in}^{-0.6})^5} Ra_{L.i} \tag{21}$$

For $10^2 \leqslant Ra_{C.i} \leqslant 10^7$

where $Ra_{L.i}$ = Rayleigh number evaluated at L_C. $L_C = (d_{g\text{-}in} - d_{r\text{-}ou})/2$. The air properties are calculated at average temperature $(t_{r.i} + t_{g.i})/2$.

2.4.2.2. Radiation heat transfer. In calculating radiation heat transfer, some assumptions are made for simplification: both the glass and selective coatings are gray, the glass is opaque to infrared radiation [5].

If the view factor between glass "i" node and absorber "i" node is considered to be one, the radiation heat transfer is expressed as below:

$$Q_{r\text{-}g.rad.i} = \frac{\sigma(t_{r.i}^4 - t_{g.i}^4)}{\frac{1-\varepsilon_{g.i}}{A_{g.rad.i}\varepsilon_{gi}} + \frac{1}{A_{r.rad.i}} + \frac{1-\varepsilon_{r.i}}{A_{r.rad.i}\varepsilon_{r.i}}} \tag{22}$$

When radiation between "i" node and n nodes before and after the "i" node is analyzed, the heat transfer can be calculated by Eqs. (23) and (24). The adjacent nodes radiation for absorber such as absorber "i-1" node and absorber "i" is zero because outer surface of absorber is convex, however it is not to glass cover due to its concave inner surface.For "i" node of the absorber tube:

$$Q_{r\text{-}g.rad.i} = \sum_{j=i-n}^{2n+1} \frac{\sigma(t_{r.i}^4 - t_{g.j}^4)}{\frac{1-\varepsilon_{g.j}}{A_{g.rad.j}\varepsilon_{g.j}} + \frac{1}{A_{r.rad.i}F_{r\text{-}i.g\text{-}j}} + \frac{1-\varepsilon_{r.i}}{A_{r.rad.i}\varepsilon_{r.i}}} \tag{23}$$

For "i" node of the glass tube:

$$Q_{r\text{-}g.rad.i} = \sum_{j=i-n}^{2n+1} \frac{\sigma(t_{r.j}^4 - t_{g.i}^4)}{\frac{1-\varepsilon_{g.i}}{A_{g.rad.i}\varepsilon_{g.i}} + \frac{1}{A_{r.rad.j}F_{r\text{-}j.g\text{-}i}} + \frac{1-\varepsilon_{r.j}}{A_{r.rad.j}\varepsilon_{r.j}}} + \sum_{j=i-n}^{2n+1} \frac{\sigma(t_{g.j}^4 - t_{g.i}^4)}{\frac{1-\varepsilon_{g.i}}{A_{g.rad.i}\varepsilon_{g.i}} + \frac{1}{A_{g.rad.j}F_{g\text{-}j.g\text{-}i}} + \frac{1-\varepsilon_{g.j}}{A_{g.rad.j}\varepsilon_{g.j}}} \tag{24}$$

where the view factors are given by [4,21].

2.4.3. Conduction through the support brackets

The brackets are used to support receiver at the focal line of a PTC and are installed at the end of receiver (see Fig. 1). The size of brackets for the SNL experiment [2] is given by [4,5]. This paper regards the brackets as fins and conduction heat loss is shown as [22]:

$$Q_{r\text{-}b.cond} = \sqrt{h_b U_b \lambda_b A_b}(t_{b0} - t_a)\text{th}\left(\sqrt{\frac{h_b U_b}{\lambda_b A_b}} l_b\right) \tag{25}$$

where h_b is the convective heat transfer coefficient and is calculated by Section 2.4.4.1.

2.4.4. Heat transfer between the glass and the ambient

There are convection and radiation heat losses from glass to the ambient. The convection can be forced or natural if there is wind or not. The radiation occurs between glass and sky because of the temperature difference between them.

2.4.4.1. Convection heat transfer. The convection heat transfer between the glass cover outer surface and ambient is given below:

$$Q_{g\text{-}a.conv.i} = \pi \Delta l \lambda_{g\text{-}a.i} Nu_{g\text{-}a.i} (t_{g.i} - t_a) \tag{26}$$

where $\lambda_{g\text{-}a.i}$ = thermal conductivity of air at $(t_{g.i}\text{-}t_a)/2$.

(A) Wind

The convection is forced when there is wind, and the correlation to estimate $Nu_{g\text{-}a.i}$ is shown as [5,23]:

$$Nu_{g\text{-}a.i} = C Re_{a.i}^m Pr_{a.i}^n \left(\frac{Pr_{a.i}}{Pr_{g.i}}\right)^{0.25} \tag{27}$$

For $0.7 < Pr_{a.i} < 500$ and $1 < Re_{a.i} < 10^6$

where $n = 0.37$ for $Pr \leqslant 10$ and $n = 0.36$ for $Pr > 10$. The correlation parameters C and m are given by Table 2. $Pr_{g.i}$ is evaluated at

outer surface temperature of the glass, and all other parameters are evaluated at the ambient temperature t_a.

(B) No wind

If there is no wind, the correlation to calculate $Nu_{g\text{-}a.i}$ is given by [5,16,24]:

$$Nu_{g\text{-}a.i} = \left\{ 0.6 + \frac{0.387 Ra_{g\text{-}a.i}^{1/6}}{\left[1 + (0.559/Pr_{g\text{-}a.i})^{9/16}\right]^{8/27}} \right\}^2 \tag{28}$$

$$Ra_{g\text{-}a.i} = \frac{g\beta_{g\text{-}a.i}(t_{g.i} - t_a)d_{g\text{-}ou}^3}{\alpha_{g\text{-}a.i}\nu_{g\text{-}a.i}} \tag{29}$$

$$\beta_{g\text{-}a.i} = 1/t_{g\text{-}a.i} \tag{30}$$

$$Pr_{g\text{-}a.i} = \nu_{g\text{-}a.i}/\alpha_{g\text{-}a.i} \tag{31}$$

For $10^5 < Ra_{g\text{-}a.i} < 10^{12}$

where air properties are calculated at average temperature $t_{g\text{-}a.i} = (t_{g.i} + t_a)/2$.

2.4.4.2. Radiation heat transfer. The solar incident radiation will be discussed in Section 2.4.5. In this section, the radiation heat transfer is due to temperature difference between glass cover and the sky. It is assumed that the glass tube is a small convex gray object in a large blackbody cavity (the sky), and the net radiation is evaluated as [5,6,11]:

$$Q_{g\text{-}s.rad.i} = \sigma\pi d_{g\text{-}ou}\Delta l\varepsilon_{g.i}(t_{g.i}^4 - t_s^4) \tag{32}$$

where the effective sky temperature t_s is evaluated to be 8 °C below atmospheric temperature t_a.

Table 2
Parameters for equation (27).

$Re_{a.i}$	C	m
1–40	0.75	0.4
40–1000	0.51	0.5
1000–200,000	0.26	0.6
200,000–1,000,000	0.076	0.7

2.4.5. Solar irradiation absorption

The solar irradiation is affected by optical properties, which are shown in Table 3:

The solar irradiation absorption of the glass cover and the absorber tube are expressed as:

$$W_{g.i} = \eta_1\eta_2\eta_3\eta_4\eta_5\eta_6\rho_c K \cdot \alpha_g \cdot I_i \tag{33}$$

$$W_{r.i} = \eta_1\eta_2\eta_3\eta_4\eta_5\eta_6\rho_c K \cdot \tau_g \cdot \alpha_r \cdot I_i \tag{34}$$

where K is equal to one when the incident angel is zero, given by [2].

2.4.6. Conduction heat transfer between inner and outer surface of the tube

When the heat conduction between inner and outer surface of pipe (absorber or glass) is considered, the equation is given by [11,12]:

$$Q_{cond.in\text{-}ou.i} = \frac{2\pi\lambda_i}{\ln(d_{ou}/d_{in})}\Delta l(t_{in.i} - t_{ou.i}) \tag{35}$$

3. Numerical solution and validation

According to Section 1, various heat transfer mathematical models established by different scholars were not exactly the same although they were all based on energy balance. The details difference will be discussed in the following.

All 1-D models for a PTC are based on Eqs. (4)–(6), however they are varied in some details making them different sharply in complexity and precision. When the length of a PTC is divided into N segments, there will be N control volumes for each of glass, absorber and fluid. Thus we will get N sets of Eqs. (4)–(6). The total control equations number is 3 × N about temperature of glass, absorber and fluid (such as [3]). If the heat conduction between the inner and outer face of glass and absorber is considered, the number of control volumes will be N for each of glass inner surface, glass outer surface, absorber inner surface, absorber outer surface and fluid. Therefore the control equations are 5 × N (such as 2-D model in [5]). These "details" are given by Table 4 and will be analyzed in Section 4.

In addition, the heat exchange terms in Eqs. (4)–(6) are slightly different in various models. In this paper, it focuses on the

Table 3
Optical properties terms [2,4–6].

η_1 Receiver shadowing (bellows, shielding, supports)		0.974	
η_2 Tracking error		0.994	
η_3 Geometry error of mirror		0.98	
ρ_c Clean mirror reflectivity		0.935	
η_4 Dirt on mirror (reflectivity is usually between 0.88 and 0.93)		Reflectivity/ρ_c	
η_5 Dirt on HCE		$(1 + \eta_4)/2$	
η_6 Unaccounted		0.96	
Selective coating	Envelope transmittance	Coating absorptance	Coating emittance
Black chrome	0.95	0.95	0.24 @300 °C
Cermet	0.95	0.96	0.14 @350 °C

Table 4
Differences of the 1-D models.

	The number of segments along length	Calculate heat conduction between the adjacent nodes	Calculate heat conduction between the inner and outer face of glass and absorber	The number of control equations
Model 1 (M 1)	N	No	No	3 × N
Model 2 (M 2)	N	Yes	No	3 × N
Model 3 (M 3)	N	No	Yes	5 × N
Model 4 (M 4)	1	No	No	3 (such as 1-D model in [5])

radiation calculation in the annulus and heat conduction through support brackets. The differences for diverse models are shown in Table 5.

The algorithm to solve the control equations is presented below for example, not considering the heat conduction between the inner and outer face of glass and absorber. Analyzing the temperature difference of internal and external surface of glass and absorber, we can adjust the algorithm in several aspects. We use the inner face temperature of absorber to calculate the convection between working fluid and absorber, however use the outer face temperature of absorber to discuss the convection and radiation in the annulus.

Table 5
Heat interactions differences in calculation.

	Consider heat loss through bracket support	Radiation calculation between absorber and glass
Model a (M a)	No (such as [2])	By Eq. (22)
Model b (M b)	Yes (such as [5])	By Eq. (22) (such as [6])
Model c (M c)	No	By Eqs. (23) and (24) (such as [4])
Model d (M d)	Yes	By Eqs. (23) and (24)

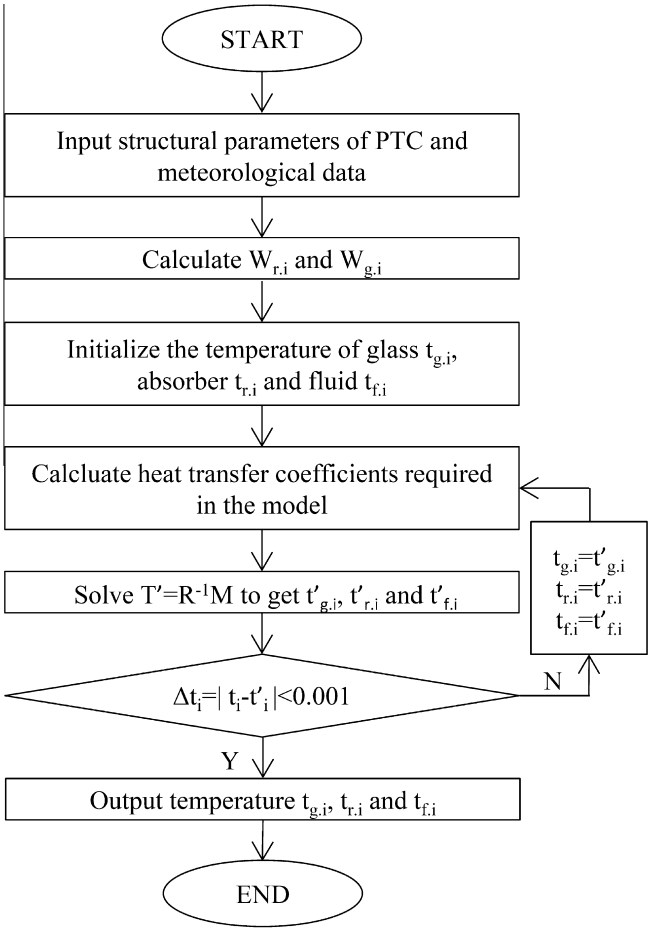

Fig. 5. Flow chart of model algorithm.

Solar irradiation absorption is independent of temperature, thus can be considered constant. Other heat transfer interactions involved in Eqs. (4)–(6) are linear relationship with temperature except radiation discussed in Sections 2.4.2.2 and 2.4.4.2. The radiation heat transfer is proportional to temperature to the fourth power and therefore make Eqs. (4)–(6) difficult to solve. In order to make Eqs. (4)–(6) linear, $h_{1,i}$ and $h_{2,i}$ are respectively defined to $h_{1,i} = Q_{r\text{-}g.rad,i}/(t_{r,i} - t_{g,i})$ and $h_{2,i} = Q_{g\text{-}s.rad,i}/(t_{g,i} - t_a)$.

Initializing temperature for glass $t_{g,i}$, absorber $t_{r,i}$ and heat transfer fluid $t_{f,i}$, the heat transfer coefficients and thermophysical parameters required in Eqs. (4)–(6) can be calculated (including $h_{1,i}$ and $h_{2,i}$). The radiation terms $Q_{r\text{-}g.rad,i}$ and $Q_{g\text{-}s.rad,i}$ can be calculated by $Q_{r\text{-}g.rad,i} = h_{1,i}\cdot(t'_{r,i} - t'_{g,i})$ and $Q_{g\text{-}s.rad,i} = h_{2,i}\cdot(t'_{g,i} - t_a)$. Thus the $3 \times N$ equations are being linear. If the coefficient, constant, and temperature matrix are respectively R, M and T, the relationship can be written as $R \times T = M$. Hence the new $t'_{g,i}$, $t'_{r,i}$ and $t'_{f,i}$ will be calculated. If the temperature error of t_i and t'_i is small enough, the initial temperature $t_{g,i}$, $t_{r,i}$ and $t_{f,i}$ are considered true. The flow chart of this model algorithm is shown in Fig. 5.

In this paper, the models are validated and analyzed with experiment data "Cermet Selective Coating – Vacuum Annulus" in [2], summarized in Table 6.

4. Results and discussion

The suitable length of each segment for "Model 1, 2 and 3" will be decided. When the control volume length is less than 0.1 m, the difference between simulated result and experiment data is almost constant. Therefore $\Delta l = 0.1$ m is decided in the analysis. The grid independent test is given by "Model 1a" based on case 1 (shown in Fig. 6) for example.

The comparison among "Model 1, 2 and 3" based on "Model a, b, c, d" is shown in Fig. 7–10. The maximum average simulated efficiency difference of "Model 1", "Model 2" and "Model 3" is 0.0375% for "Model a", 0.0374% for "Model b", 0.0430% for "Model c" and 0.0431% for "Model d" respectively. Hence it is unnecessary to consider the heat conduction between the inner and outer face of the glass tube and absorber pipe, as well as the neighboring nodes along with the length. It focuses on "Model 1" and "Model 4" below.

Considering the influence of dividing a HCE into N segments along the length except other factors, "Model 1and 4" are compared on the basis of "Model a" as shown in Fig. 11. The differences of the simulated results are 0.002 °C in outlet temperature and 0.01% in efficiency when the receiver is 10 m. However the

Table 6
Test data for SEGS LS-2 solar collector [2].

	Direct normal insolation (W/m^2)	Wind speed (m/s)	Air temperature (°C)	Temperature in (°C)	Temperature out (°C)	Flow rate (L/min)	Measured efficiency (%)	Est error (%)
Case 1	933.7	2.6	21.2	102.2	124.0	47.7	72.51	1.95
Case 2	968.2	3.7	22.4	151.0	173.3	47.8	70.9	1.92
Case 3	982.3	2.5	24.3	197.5	219.5	49.1	70.17	1.81
Case 4	909.5	3.3	26.2	250.7	269.4	54.7	70.25	1.90
Case 5	937.9	1.0	28.8	297.8	316.9	55.5	67.98	1.86
Case 6	880.6	2.9	27.5	299.0	317.2	55.6	68.92	2.06
Case 7	920.9	2.6	29.5	379.5	398.0	56.8	62.34	2.41
Case 8	903.2	4.2	31.1	355.9	374.0	56.3	63.82	2.36

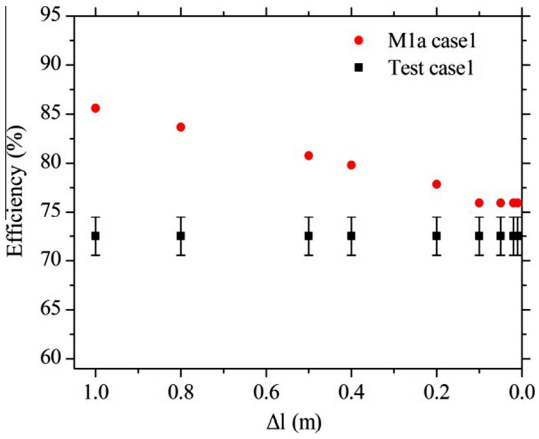

Fig. 6. Grid independent test.

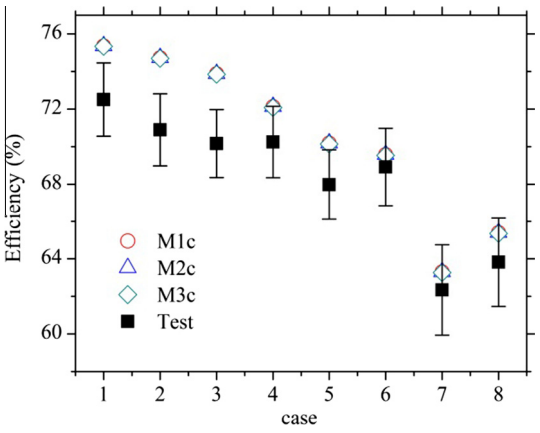

Fig. 9. Comparison among Model 1, 2 and 3 based on Model c.

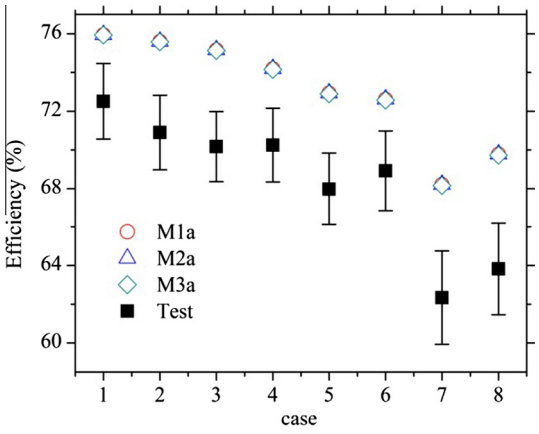

Fig. 7. Comparison among Model 1, 2 and 3 based on Model a.

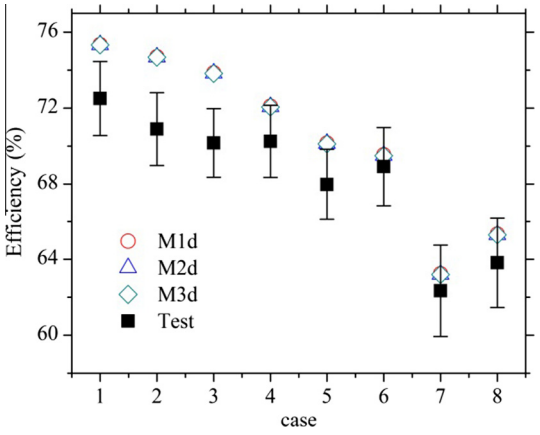

Fig. 10. Comparison among Model 1, 2 and 3 based on Model d.

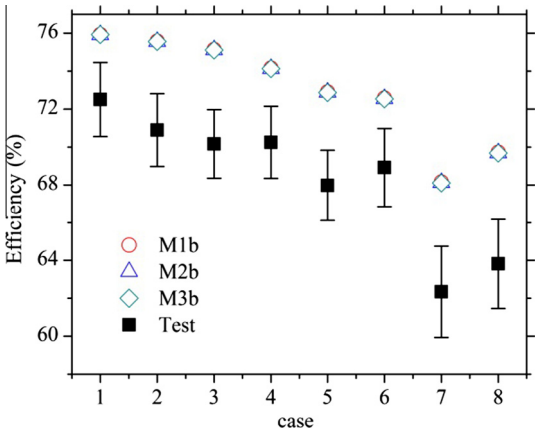

Fig. 8. Comparison among Model 1, 2 and 3 based on Model b.

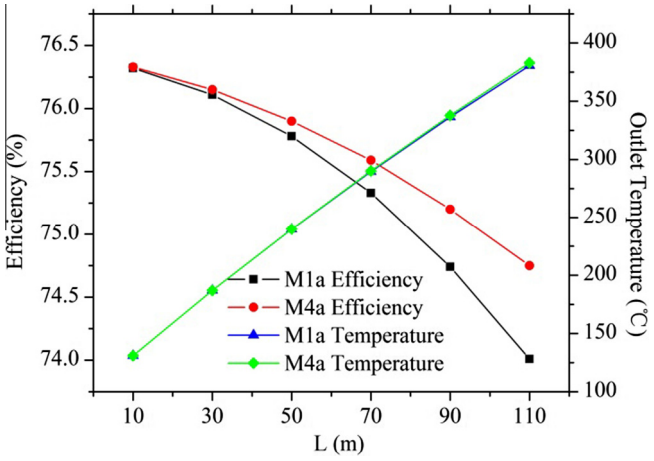

Fig. 11. Comparison between Model 1a and 4a with length increasing (based on case 1).

advantage of "Model 1" is gradually obvious with the length increasing, they are 2.51 °C and 0.75% at 110 meters long. Thus dividing control volumes along length is necessary when the HCE is especially long.

The influence of heat conduction through bracket support and radiation calculation in the annulus is given by Fig. 12. It is obvious that the model precision significantly improves when the radiation between the adjacent elements is considered. The precision increases when the bracket support heat loss is added, however it is far less than improving the radiation in the annulus. In this paper cases, the average improvements of precision are 0.03% in efficiency and 0.01 °C in temperature for calculating the bracket support heat loss, but they are 2.48% and 0.7 °C for improving the radiation.

Summarized in Fig. 13 based on case 1, the temperature and the efficiency difference are 6.58 °C and 1.95% between "Model 1a and

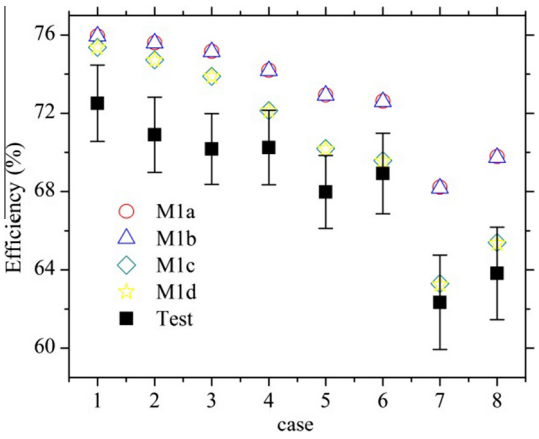

Fig. 12. Comparison among Model a, b, c and d based on Model 1.

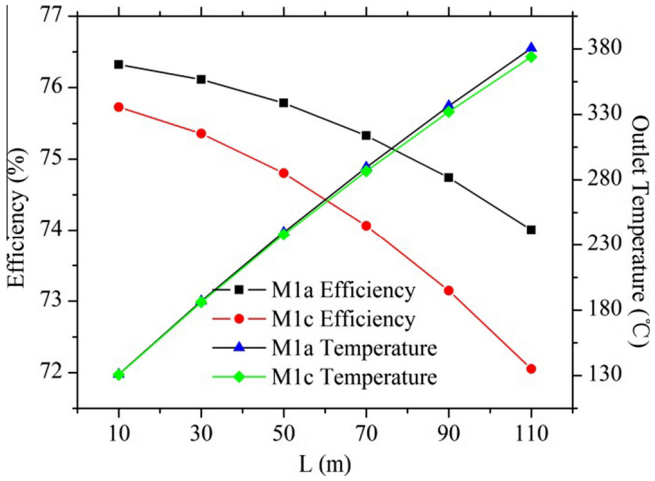

Fig. 13. Comparison between Model 1a and Model 1c with length increasing (based on case 1).

Table 7
Outlet temperature and heat gain comparison [2,13].

	Test		Model 1d		Results in [13]	
	Temperature (°C)	Heat gain (kW)	Temperature (°C)	Heat gain (kW)	Temperature (°C)	Heat gain (kW)
Case 1	124.0	26.44	124.9	27.58	126.2	29.14
Case 2	173.3	26.95	174.5	28.36	177.0	31.48
Case 3	219.5	26.99	220.7	28.45	222.8	31.08
Case 4	269.4	24.92	270.0	25.71	272.4	28.96
Case 5	316.9	25.00	317.5	25.80	318.4	26.98
Case 6	317.2	23.83	317.3	24.01	319.9	27.40
Case 7	398.0	22.55	398.2	22.83	400.4	25.50

1c" when the HCE length is 110 m, which is more than those in Fig. 11. Thus, it is more important to consider the neighboring nodes radiation in simulation when the HCE is long.

In [13], the 3-D model was established, and their simulated results were validated with case 1–7 adopted by this paper. The comparison among the experiment [2], the "Model 1d" (the most precise model in this paper) and the results [13] are presented by Table 7. The 1-D "Model 1d" seems to be more precise than the 3-D model from the simulated results. The reason may be that there are more assumptions for 3-D model than the 1-D one, therefore the error is bigger. The simulated temperature and efficiency by this paper are a little higher than the experiment results. This consequence may be caused by neglecting some heat loss such as the end heat conduction. The model prediction gave rather large error in some cases, and this may be due to experiment error.

5. Conclusion

This paper focuses on the 1-D models for PTCs under different assumptions and details, considering all the heat transfer processes. A simple algorithm is adopted to solve the non-linear equations easily. These 1-D models are compared with each other, and validated with the test data from Sandia National Laboratories. A 1-D model may be more accurate, but more complicated. It can choose an appropriate 1-D model under a certain condition. If the HCE is not too long, it is unnecessary to divide its length into N segments in modeling. The simulated efficiency and outlet temperature difference are 0.75% and 2.51 °C at 110 m between models dividing the length and not. The heat conduction from inner face to outer face of the glass tube, absorber pipe and the adjacent nodes along the length can be neglected. The maximum simulated efficiency difference between models considering the heat conduction and not is 0.0431%. The radiation in the annulus between the neighboring control volumes along the length must be considered because it can improve the model accuracy greatly, especially when the HCE is long. The simulating difference is 1.95% in efficiency and 6.58 °C in outlet temperature at 110 m between models calculating radiation of adjacent nodes along the length and not. The 1-D models established in this paper are precise enough compared with the 3-D model from other research and the experiment data. The average simulated outlet temperature of the most accurate model in this paper is 0.65 °C higher than the test data, however it is 2.69 °C higher for the 3-D model than the experiment results. Besides the 1-D models are more simplified than the 3-D model. In conclusion, the 1-D models established in this paper can be used to investigate the thermal performance of the PTC in the future.

Acknowledgement

This work is supported by the National Science and Technology Program project of China's twelfth five-year plan in rural areas (2011BAJ08B08-2).

References

[1] Fernández-García A, Zarza E, Valenzuela L, Pérez M. Parabolic-trough solar collectors and their applications. Renew Sust Energ Rev 2010;14:1695–721.
[2] Dudley VE, Kolb GJ, Sloan M, Kearney D. Test Results: SEGS LS-2 Solar Collector. Report of Sandia National Laboratories (SAND94-1884); 1994.
[3] Ouagued M, Khellaf A, Loukarfi L. Estimation of the temperature, heat gain and heat loss by solar parabolic trough collector under Algerian climate using different thermal oils. Energ Convers Manage 2013;75:191–201.
[4] Padilla RV, Demirkaya G, Goswami DY, Stefanakos E, Rahman MM. Heat transfer analysis of parabolic trough solar receiver. Appl Energ 2011;88:5097–110.
[5] Forristall R. Heat transfer analysis and modeling of a parabolic trough solar receiver implemented in engineering equation solver. NREL/TP-550-34169; October 2003.
[6] Kalogirou SA. A detailed thermal model of a parabolic trough collector receiver. Energy 2012;48:298–306.
[7] Odeh SD, Morrison GL, Behnia M. Modelling of parabolic trough direct steam generation solar collectors. Sol Energy 1998;62(6):395–406.
[8] Kassem T. Numerical study of the natural convection process in the parabolic–cylindrical solar collector. Desalination 2007;209:144–50.
[9] Li J, Wang ZF, Lei DQ, Li JB. Hydrogen permeation model of parabolic trough receiver tube. Sol Energy 2012;86:1187–96.
[10] Liu QB, Yang ML, Lei J, Jin HG, Gao ZC, Wang YL. Modeling and optimizing parabolic trough solar collector systems using the least squares support vector machine method. Sol Energy 2012;86:1973–80.

[11] Gong GJ, Huang XY, Wang J, Hao ML. An optimized model and test of the China's first high temperature parabolic trough solar receiver. Sol Energy 2010;84:2230–45.
[12] Lu JF, Ding J, Yang JP, Yang XX. Nonuniform heat transfer model and performance of parabolic trough solar receiver. Energy 2013;59:666–75.
[13] He YL, Xiao J, Cheng ZD, Tao YB. A MCRT and FVM coupled simulation method for energy conversion process in parabolic trough solar collector. Renew Energ 2011;36:976–85.
[14] Cheng ZD, He YL, Cui FQ, Xu RJ, Tao YB. Numerical simulation of a parabolic trough solar collector with nonuniform solar flux conditions by coupling FVM and MCRT method. Sol Energy 2012;86:1770–84.
[15] Wu ZY, Li SD, Yuan GF, Lei DQ, Wang ZF. Three-dimensional numerical study of heat transfer characteristics of parabolic trough receiver. Appl Energ 2014;113:902–11.
[16] Hachicha AA, Rodríguez I, Capdevila R, Oliva A. Heat transfer analysis and numerical simulation of a parabolic trough solar collector. Appl Energ 2013;111:581–92.
[17] Gnielinski V. New equations for heat and mass transfer in turbulent pipe and channel flow. Int Chem Eng 1976;16(2):359–63.
[18] Ratzel A, Hickox C, Gartling D. Techniques for reducing thermal conduction and natural convection heat losses in annular receiver geometries. J Heat Trans 1979;101:108–13.
[19] Marshal N. Gas Encyclopedia. New York: Elsevier; 1976.
[20] Raithby GD, Hollands K. A general method of obtaining approximate solutions to laminar and turbulent free convection problems. Adv Heat Transf 1975;11:265–315.
[21] Yang XR, Ma QF, Yuan GX, Fang RS, Yang YH. Handbook of radiation view factors. Beijing: National Defense Industry Press; 1982 [In Chinese].
[22] Zhang XM, Ren ZP, Mei FM. Heat transfer theory. 5th ed. Beijing: China Building Industry Press; 2007 [In Chinese].
[23] Incropera F, DeWitt D. Fundamentals of heat and mass transfer, 3rd ed; 1990.
[24] Churchill S, Chu H. Correlating equations for laminar and turbulent free convection from a horizontal cylinder. Int J Heat Mass Trans 1975;18(9):1049–53.